polymers

MDPI

Article

Preparation and Performance of Supercritical Carbon Dioxide Thickener

Bin Liu, Yanling Wang * and Lei Liang

School of Petroleum Engineering, China University of Petroleum (East China), Qingdao 266580, China; B19020038@s.upc.edu.cn (B.L.); jerryleon1224@outlook.com (L.L.)
* Correspondence: wangyl@upc.edu.cn

Abstract: The low sand-carrying problem caused by the low viscosity of supercritical carbon dioxide (SC–CO_2) limits the development of supercritical CO_2 fracturing technology. In this study, a molecular simulation method was used to design a fluorine-free solvent-free SC–CO_2 thickener 1,3,5,7-tetramethylcyclotetrasiloxane (HBD). Simulations and experiments mutually confirm that HBD-1 and HBD-2 have excellent solubility in SC–CO_2. The apparent viscosity of SC–CO_2 after thickening was evaluated with a self-designed and assembled capillary viscometer. The results show that when the concentration of HBD-2 is 5 wt.% (305.15 K, 10 MPa), the viscosity of SC–CO_2 increases to 4.48 mPa·s. Combined with the capillary viscometer and core displacement device, the low damage of SC–CO_2 fracturing fluid to the formation was studied. This work solves the pollution problems of fluoropolymers and co-solvents to organisms and the environment and provides new ideas for the molecular design and research of SC–CO_2 thickeners.

Keywords: supercritical carbon dioxide; thickener; molecular simulation; core damage; greenhouse effect

Citation: Liu, B.; Wang, Y.; Liang, L. Preparation and Performance of Supercritical Carbon Dioxide Thickener. *Polymers* **2021**, *13*, 78. https://doi.org/10.3390/polym13010078

Received: 30 November 2020
Accepted: 22 December 2020
Published: 28 December 2020

1. Introduction

In shale gas hydraulic fracturing, water is an important resource. However, with the continuous application of hydraulic fracturing technology, problems such as water scarcity, drinking water pollution, and flowback water treatment have gradually become prominent [1]. Researchers began to focus on supercritical carbon dioxide (SC–CO_2) fracturing fluid technology. Richard S. [1,2] systematically studied the pros and cons of using CO_2 as the working fluid for shale gas production: (1) CO_2 fracturing effect and fracture expansion are better than water-based hydraulic fracturing, and under constant pressure test conditions on the shale surface CO_2 adsorption is better than CH_4 at elevated temperature, which facilitates gas extraction and also serves as a fixation of CO_2 [3] show in Figure 1, (2) Possible shortcomings, including the cost and safety issues related to handling a large amount of SC–CO_2: separation of CO_2 and CH_4 mixed gas, transportation costs, pressure safety, and other issues. SC–CO_2 has the characteristics of high diffusion coefficient, ultra-low surface tension, and strong permeability. SC–CO_2 injection into shale changes the pore characteristics of shale, reduces the specific surface area, increases the porosity and average pore size, and improves the fracturing effect [4]. SC–CO_2 fracturing technology can solve the shortcomings of water-based fracturing fluid systems such as large waste of water resources, clay swelling, and residual working fluid that cause damage to the reservoir and incomplete reverse drainage to cause groundwater pollution [5–7].

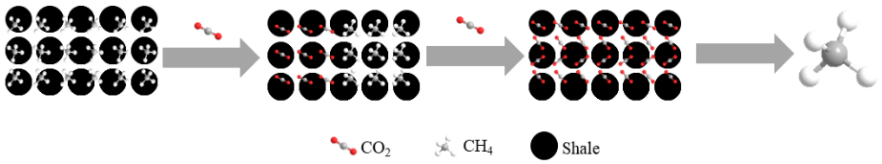

Figure 1. Capturing CO_2 while extracting gas (competitive adsorption of CO_2 and CH_4).

According to existed research, the advantages of fluoropolymers [8] in chemistry and low surface tension make them widely used in the area of oil field chemistry. The reported fluoropolymers [9–11] generally have an excellent performance in SC–CO_2 thickening, but fluorine-containing monomers are expensive. Fluorine was widely used in aerospace, petroleum, chemical, and other areas. It flows into the water cycle through wastewater discharge, and it cannot be metabolized and is enriched in biological extraction, causing great harm [12]. The reported siloxane thickeners [13–17] rely on the formation of Lewis acid hydrogen bonds between the cosolvent and CO_2 and the similar compatibility of the cosolvent with siloxane to enhance solubility. Silicone has the characteristics of the low glass transition temperature, low cohesive energy, and good economy. Modified silicone thickeners have great development potential. The reported hydrocarbon thickener [18,19]: (1) Low-molecular-weight compounds have good solubility in CO_2 and poor thickening effect, (2) Long-chain polymer hydrocarbons are soluble in CO_2 under co-solvent conditions, but the damage of co-solvents to the formation cannot be ignored [14]. In this work, we designed and prepared two environmentally friendly supercritical carbon dioxide thickeners, which solved the problem of high cost and high pollution caused by the use of fluoropolymer and cosolvent in the past. Moreover, the thickener has excellent solubility and thickening performance and has certain temperature resistance and pressure resistance.

A self-designed high-precision capillary viscometer was used to measure the apparent viscosity of the CO_2 fracturing fluid after thickening; the capillary viscometer was used in conjunction with a core displacement device to study core damage and fluid loss. In addition, the contents of different thickeners, the influence of temperature, pressure, and concentration on CO_2 viscosity, combined with Materials Studio and Abaqus to study the solubility, thickening mechanism, and fracturing simulation respectively.

2. Materials and Methods

2.1. Materials Studio Simulation

The polymer simulated in this paper was named HBD-1 and HBD-2, and a CO_2 system with 1000 CO_2 molecules, a polymer system with 4 polymer chains, and a polymer with 4 polymer chains 1000 CO_2 molecules were established by using the Material Studio software (Accelrys Ltd., San Diego, CA, USA), the all-atom molecular model of CO_2 system, as shown in Figure 2.

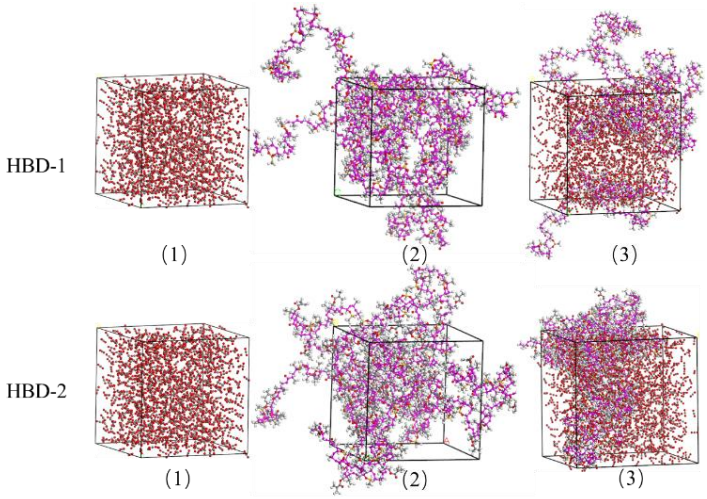

Figure 2. Three kinds of systems established by all-atom molecular model of HBD-1 and HBD-2. (**1**) The CO_2 system with 1000 CO_2 molecules; (**2**) the polymer systems with 4 polymer chains; (**3**) the polymer-CO_2 systems with 4 polymer chains and 1000 CO_2 molecules.

After the Forcite optimization and annealing calculation of the amorphous cell module, MD simulation of the amorphous cell module was carried out in the NPT system. The temperature was set to 305.15 K, and the temperature was set to 0.01 GPa. The running time for all the systems was 400 ps, and the trajectories were saved at 1 ps intervals [20–22].

2.2. Synthesis and Characterization of the Hyperbranched D4H

The materials used in the experiment were ethylene glycol dimethacrylate, 2,4,6,8-tetramethylcyclotetrasiloxane (D4H), trimethylolpropane trimethacrylate and $H_2PtCl_6{\cdot}6H_2O$, which were purchased from Macleans. HBD-1 and HBD-2 were synthesized by hydrosilylation [23] according to the procedure shown in Scheme 1.

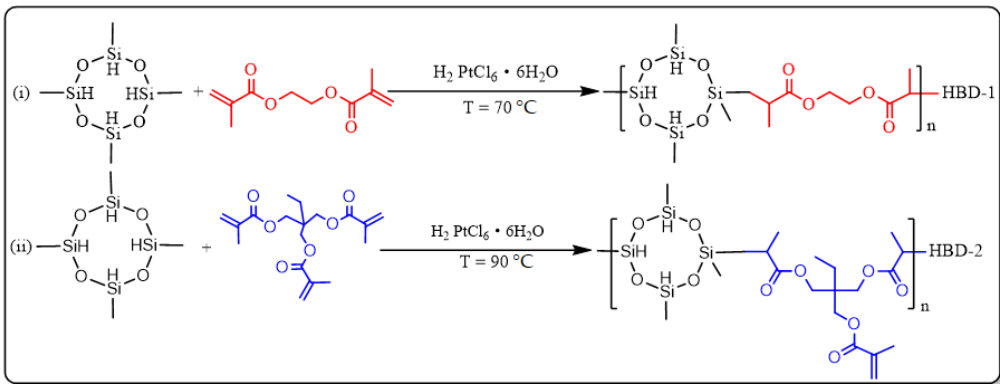

Scheme 1. Synthetic routes of HBD-1 and HBD-2.

Ethylene glycol dimethacrylate was washed with 1–5% NaOH alkali solution for three times to remove MEHQ, and then washed for three times to remove NaOH. Anhydrous magnesium sulfate was dried, filtered to remove magnesium sulfate, distilled to remove the remaining alkali, and then refrigerated at low temperatures. First, 16.4833 g of ethylene glycol dimethacrylate was added to a 250 mL three-necked flask under magnetic stirring. When the solution temperature rises to 70 °C, 40 ppm catalyst was added to activate for 2 h. Then 10 g of D4H (2,4,6,8-tetramethylcyclotetrasiloxane) was slowly dropped into a three-mouth bottle (about 30 min~35 min), and HBD-1 initial product was obtained after 4 h reaction. To remove chloroplatinic acid, 1 g activated carbon was added into the product, and the mixture was repeatedly washed with distilled water after hydrosilylation

was stopped. Under the vacuum conditions of 370 K and 0.06 MPa, the small molecule compounds and water were removed by the rotating evaporator. At 90 °C, the ethylene glycol dimethacrylate was replaced by 16.8841 g trimethylolpropane trimethacrylate to produce HBD-2.

2.2.1. H NMR Measurements

Bruker-400 MHz NMR (Bruker Ltd., Switzerland) was used to characterize the ^{1}H NMR spectrum of the polymer with deuterated chloroform as solvent [20,24,25].

2.2.2. FT-IR Measurements

The infrared spectrum measurement of the polymer was completed by Nicolet iS50 Fourier transforms infrared spectrometer (Thermo Fisher Scientific Ltd., Waltham, MA, USA). After washing the ATR crystal with ethanol, spread 0.10 mL of the sample evenly on the surface of the ATR. The scan number of the spectrum is 128 and the resolution is 8 cm^{-1}. The wave number ranges from 4000 to 400 cm^{-1} [26].

2.2.3. GPC Measurements

The measurement of polymer molecular weight is done by WATERS 2414 refractive index detector (Waters Ltd., Shanghai, China). Prepare 5 mg/mL polymer solution with chromatographic grade tetrahydrofuran and pass the solution through the gel chromatography column at a flow rate of 1 mL/min at 35 °C [27].

2.2.4. Differential Scanning Calorimetry

The glass transition temperature of the polymer was measured using a Mettler-Toledo differential scanning calorimeter in nitrogen atmosphere (Mettler-Toledo Co., Shanghai, China). A 10 mg polymer sample was placed on the bottom of an aluminum crucible and sealed with a porous lid. The heating rate and cooling rate are 5 °C/min. Take the average of three measurements as the result [28–30].

2.2.5. Viscosity Measurement

The capillary viscometer (Figure 3) was composed of a plunger pump, a visualization chamber, a viscosity measurement part, and a data collection terminal to study the viscosity of SC–CO_2 fracturing fluid after thickening. The inner diameter of the capillary is D = 0.8 mm First, carbon dioxide and thickener are pumped into intermediate container I through booster pump I, booster pump II, and the second ISCO pump pumps the mixed thickener and CO_2 into the visualization container, turn on the heating area to ensure that the conditions in the container reach T = 304.25 K, P = 7.38 MPa [31] (supercritical conditions) or above, and then the clarified mixed liquid was pumped into the intermediate container II and pressed into the capillary at a constant flow rate In the end, the pressure difference recorded by the differential pressure sensor at both ends of the capillary are expressed in Equation (1), which was generally suitable for laminar fluids [32].

$$\eta = \frac{\tau_w}{\gamma_w} = \frac{D\Delta p/4L}{8v/D} \quad (1)$$

where η was fluid apparent viscosity (Pa s), τ_w was wall shear stress (Pa), γ_w was the apparent shear rate (s^{-1}), D presented the capillary diameter (m), Δp was the pressure difference of capillary (MPa), and L was capillary length (m), v was the flow velocity of thickened liquid CO_2 (m s^{-1}).

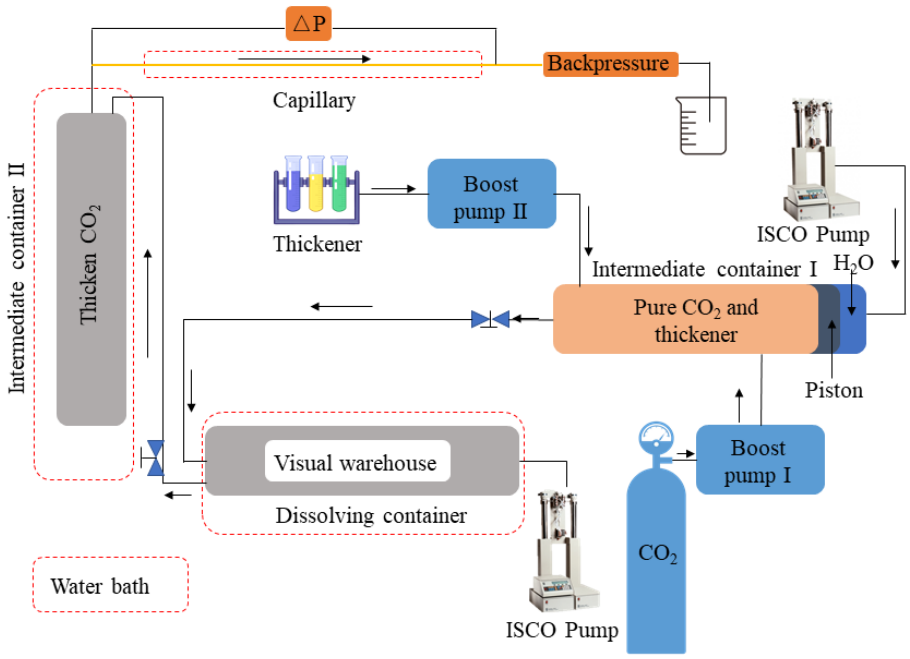

Figure 3. Capillary viscometer.

2.2.6. Cloud Point Measurement

Figure 4 was used for cloud point measurement. Before the experiment, open switch 5 to drain the air in the visualization container by a vacuum pump (the switches not mentioned in each step were closed), and the left side of the intermediate container II was filled with water. (1) 1 wt.% HBD thickener (305.15 K) was added to the visualization reactor. (2) Turn on the 1,2,6 switches, compress the CO_2 into liquid in the intermediate container I with ISCO pump, turn on switch 4 to transfer the liquid CO_2 to the visible container, and operate repeatedly until the container was filled. (3) After the thickener was mixed with CO_2, turn on switches 3 and 4, and slowly draw out the homogeneous liquid in the visible container with a hand pump to observe the cloud point phenomenon (the pressure when the homogeneous solution was turbid). In the whole experiment process, the pressure rise was controlled by ISCO pump, and the depressurization was controlled by hand pump.

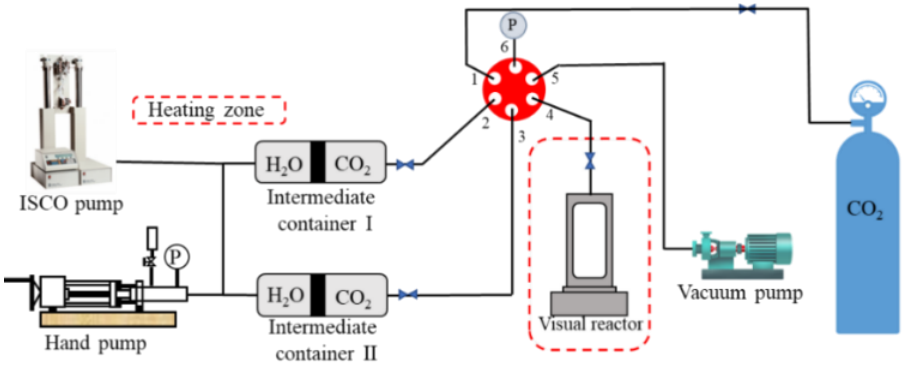

Figure 4. SC–CO_2 phase behavior evaluation device.

2.2.7. Core Damage Measurements

Before the start of the experiment, pure SC–CO_2 was injected into the core holder (Figure 5) at an injection rate of 0.181 mL/min, the pressure difference between the two sides of the core holder was recorded, and the permeability of the heterogeneous core was calculated, Equation (2). In this work, the displacement fluid is supercritical carbon dioxide.

The results show that SC–CO_2 has no damage to the core studied. After thickening, the SC–CO_2 displacement experiment was carried out at 0.18 mL/min. The specific experimental steps are as follows: (1) The initial permeability was measured by vacuum pumping and supercritical carbon dioxide saturation. (2) At a constant flow rate of 0.18 mL/min, the thickened supercritical carbon dioxide was injected to keep the fluid pressure stable in the intermediate vessel. (3) During the whole experiment, the change of injection end pressure was monitored, the backpressure was kept at 8 MPa, and the confining pressure was always 4 MPa higher than the inlet pressure. The pressure difference between the two sides of the core holder was recorded, and the permeability of the heterogeneous core after fracturing was calculated.

$$k = \frac{q\mu L}{A\Delta p} \quad (2)$$

where k was permeability (μm^2), q was flow rate (cm^3/s), μ was the viscosity (mPa·s), L presented the core length (cm), A was core cross-sectional area (cm^2), and Δp was the pressure difference of core holder (mPa).

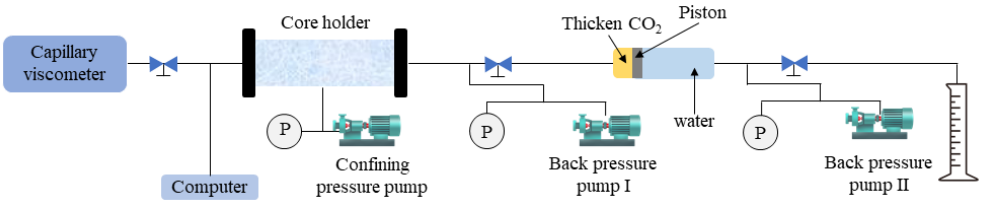

Figure 5. Core damage and fluid loss test instrument.

3. Results and Discussion

3.1. Materials Studio Computational Simulation

3.1.1. Interaction Energy Calculation

In the polymer-CO_2 system, the dissolution of the polymer in CO_2 mainly depends on the polymer-CO_2 interaction. The interaction energy (E_{inter}) can quantitatively characterize the intensity of its action. The greater the absolute value of the interaction energy was, the stronger the polymer-CO_2 interaction was. First, calculate the total energy $E_{polymer\text{-}CO2}$ of the polymer chain-CO_2 in the above stabilization, then calculate the $E_{polymer}$ and E_{CO2}(The calculation results are recorded in Table 1), and finally the interaction energy was calculated by Equation (3) [20].

$$E_{inter} = E_{polymer\text{-}CO_2} - (E_{polymer} + E_{CO_2}) \quad (3)$$

Table 1. $E_{polymer\text{-}CO_2}$, $E_{polymer}$ and E_{CO_2} parameters of HBD-1 and HBD-2.

System	$E_{polymer\text{-}CO_2}$/kJ·mol^{-1}	$E_{polymer}$/kJ·mol^{-1}	E_{CO_2}/kJ·mol^{-1}	E_{inter}/kJ·mol^{-1}
Poly HBD-1 and SC–CO_2	−4525.25	−5937.54	1910.17	−497.88
Poly HBD-2 and SC–CO_2	−4727.68	−5734.77	1910.17	−903.08

3.1.2. Cohesive Energy Density and Solubility Parameter

The cohesive energy density (CED) and solubility parameters are also generally used to represent the interaction between polymer molecules. The cohesive energy density was the energy required for vaporization of 1 mol condensate per unit volume to overcome the intermolecular force, and mainly reflects the interaction between groups. The square of the solubility parameter was the cohesive energy density. Relevant studies have shown that polymers with lower cohesive energy density have a higher solubility in CO_2 [33–35], and the smaller the difference between the solubility parameter of the polymer and CO_2 was,

the better the solubility of the polymer in CO_2 was [36]. The CED and solubility parameter (δ) of the polymer and CO_2 was shown in Table 2. The $|\Delta\delta|$ of the two systems in Table 2 are 1.08 and 0.04 respectively.It can be seen that HBD-1 and HBD-2 have good solubility in SC–CO_2.

Table 2. CED and solubility parameter values of the polymer and CO_2.

System	CED/(J/m^3)	δ/(J/cm^3)$^{1/2}$	$\|\Delta\delta\|$/(J/cm^3)$^{1/2}$
PolyHBD-1-CO_2	2.08×10^8	14.42	1.08
PolyHBD-2-CO_2	1.79×10^8	13.38	0.04
CO_2	1.78×10^8	13.34	0

$|\Delta\delta| = |\delta_{\text{Polymer-}CO_2} - \delta_{CO_2}|$.

3.1.3. Radial Distribution Function (RDF)

The mechanism of polymer solvation in SC–CO_2 was studied by comparing the RDF value of carbon atom in polymer-CO_2 with that of carbon atom in polymer-polymer. If the RDF value of polymer-CO_2 was larger, it proves that polymer HBD-1 was miscible with SC–CO_2 [20–22,37,38]. The results of the polymer-CO_2 and polymer-polymer are shown in Figure 6. The results show that the RDF value of polymer-CO_2 was greater than that of polymer-polymer, and polymer HBD-1and HBD-2 has good miscibility in SC–CO_2.

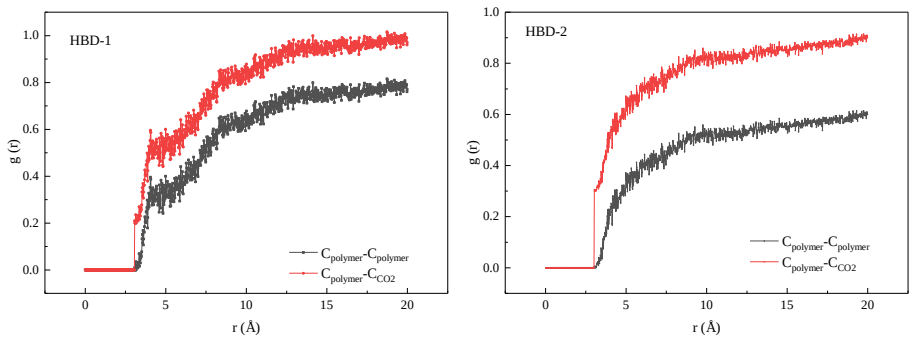

Figure 6. Radial distribution functions of the intermolecular C–C pairs for Polymer-CO_2 systems at 305.15 K and 10 Mpa.

3.2. Structural Characterization of HBD-1 and HBD-2

The FT-IR and ^{1}H NMR spectra of D4H, HBD-1, and HBD-2 were recorded in Figures 7 and 8. In the infrared spectra of D4H, HBD-1, and HBD-2, there were Si—O characteristic peaks at 1050 cm^{-1}~1100 cm^{-1} [15], and Si—C characteristic peaks at 850 cm^{-1}~890 cm^{-1}. It can be seen from Figure 8 that the Si—H peak at 2160 cm^{-1} was significantly weakened, and a C=O peak appeared at 1735 cm^{-1} [39]. In the FT-IR of HBD-2, a peak of 1635 cm^{-1} appeared. The numerical changes of these characteristic peaks indicate the changes in the functional groups corresponding to the hydrosilylation reaction. The double bond peak still exists in the infrared image of HBD-2 because the double bond is excessive in the reaction.

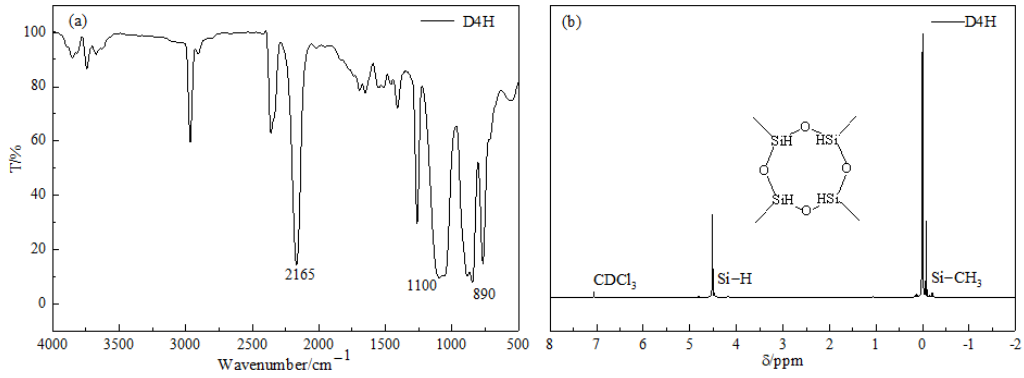

Figure 7. Structural characterization of D4H. (**a**) FT-IR spectrum of D4H, (**b**) ^{1}H NMR spectrum of D4H.

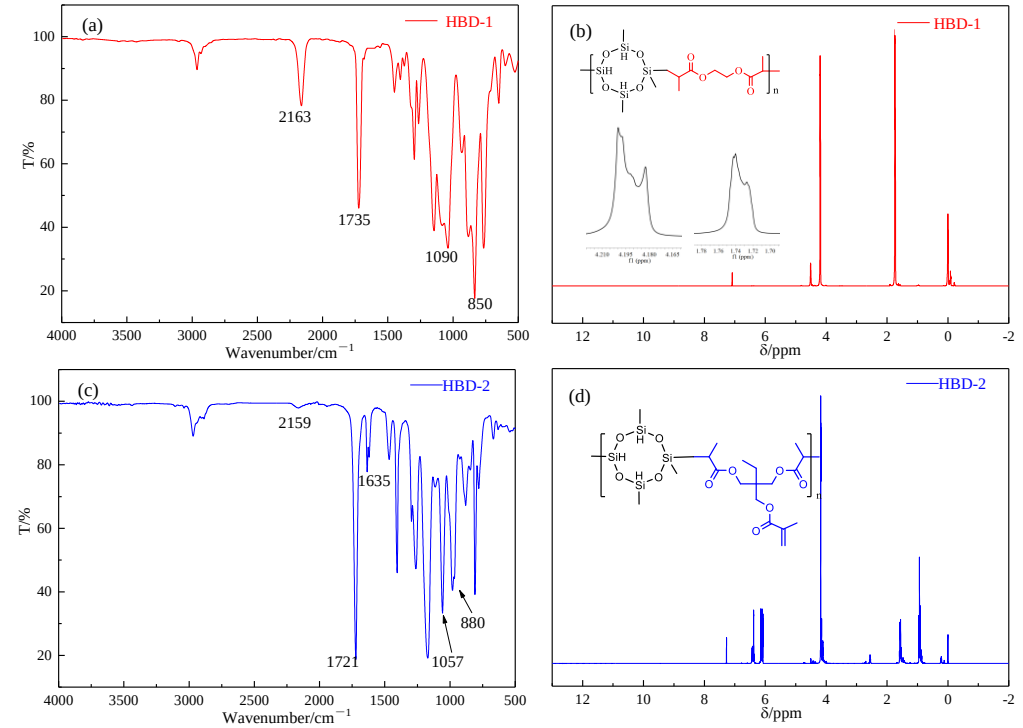

Figure 8. Structural characterization of HBD-1 and HBD-2. (**a**) FT-IR spectrum of HBD-1, (**b**) ^{1}H NMR spectrum of HBD-1, (**c**) FT-IR spectrum of HBD-2, (**d**) ^{1}H NMR spectrum of HBD-2.

The ^{1}H NMR shift data of HBD-1 and HBD-2 were shown in Table 3. It can be seen from Figure 7 that the Si–H peak in D4H appears at 4.5 ppm. In combination with Table 3, Figures 7 and 8, it can be seen that the chemical shift in the ^{1}H NMR spectrum indicates that the two polymers undergo addition reactions with two symmetrical H in D4H, so Si–H still exists in HBD-1 and HBD-2. However, there are double-bonded hydrogens at 6.02 ppm~6.4 ppm in the HBD-2 ^{1}H NMR spectrum. This is because the monomer trimethylolpropane trimethacrylate that participates in the hydrosilylation reaction contains excessive double bonds, and these double bonds do not participate in the reaction due to steric hindrance. The numerical changes of these characteristic peaks indicate the changes in the functional groups corresponding to the hydrosilylation reaction. The double bond peak still exists in the infrared image of HBD-2 because the double bond is excessive in the reaction. Combined with FT-IR and ^{1}H NMR, HBD-1 and HBD-2 were successfully prepared.

Table 3. Chemical shift of HBD-1 and HBD-2.

	δ/ppm	Type of H
HBD-1	0.19	$Si–CH_3$
	1.70–1.78	$Si–CH_2–CH–CH_3$ $O=C–CH(CH_3)–CH_2$
	4.16–4.21	$–O–CH_2–CH_2–O–$
	4.5	Si–H
	7.39	$CDCl_3$
HBD-2	0.19	$Si–CH_3$
	0.83	$(CH_2)_3–C–CH_2–CH_3$
	1.63–1.85	$(CH_2)_3–C–CH_2–CH_3$ $O=C–CH–(CH_3)_2$ $O=C–CH=CH_2$ $O=C–CH(CH_2Si)–CH_3$
	2.3–2.4	$O–C–CH–(CH_3)_2$ $O=C–CH(CH_2Si)–CH_3$
	4.15–4.23	$(CH_2)_3–C–CH_2–CH_3$
	4.5	Si–H
	6.02–6.4	$O=C–CH=CH_2$
	7.39	$CDCl_3$

3.3. Glass Transition Temperature and Molecular Weight Analysis

Figure 9a,b are the DSC and GPC spectra of HBD, respectively. It can be seen from (a) that glass transition temperature (T_g) of HBD-1 and HBD-2 is −15 °C and −44.5 °C, respectively. The T_g was generally used to characterize the relative flexibility of polymer chains, the lower the glass transition temperature was, the better the flexibility of the molecular chain was [40,41]. High polymer chain flexibility helps to dissolve HBD in SC–CO_2 [35]. The polymer parameters were shown in Table 4.

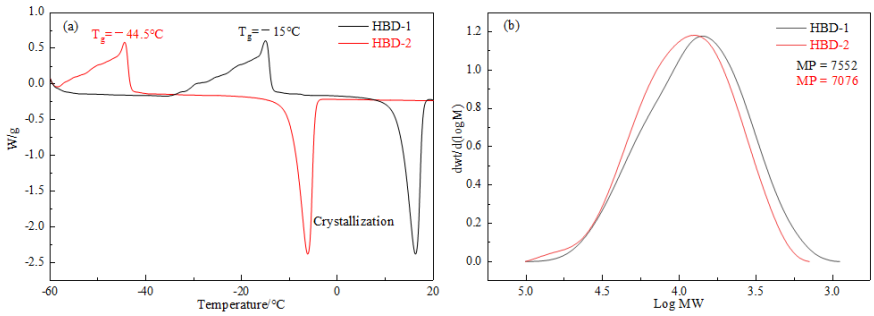

Figure 9. DSC (**a**) and GPC (**b**) characterization result.

Table 4. Polymer parameters.

	Molecular Weights (MP)	Polymerization Degree
HBD-1	7552	17
HBD-2	7076	16

3.4. Cloud Point and Viscosity of HBD-1 and HBD-2 in SC–CO_2

3.4.1. Cloud Point and Phase Behavior of HBD-1 and HBD-2 in SC–CO_2

The phase behavior system consists of thickener HBD and SC–CO_2. It can be seen that pure CO_2 was a transparent liquid (298.15 K, 7.48 MPa). In Figure 10b, HBD-1 was milky white and HBD-2 was translucent, which indicates that HBD-2 (298.15 K, 7.48 MPa) was more soluble in SC–CO_2. The experimental results of Figure 10c show that HBD-1 and HBD-2 thickeners have excellent solubility in SC–CO_2 after being kept at a constant

temperature of 305.15 K for 12 h. This was in good agreement with the results of E_{inter}, CED, and RDF. As well, the cloud point pressure of the thickener SC–CO_2 system in this study was lower than 7.48 MPa.

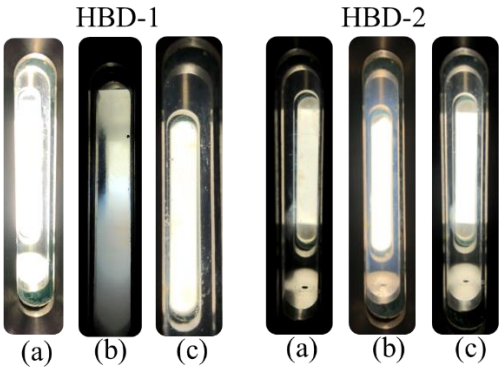

Figure 10. Phase behavior of HBD-1 and HBD-2 (**a**) pure CO_2 at 298.15 K and 7.48 MPa (**b**) 1 wt.% thickened SC–CO_2 at 298.15 K and 7.48 MPa (**c**) 1 wt.% thickened SC–CO_2 at 305.15 K and 7.48 MPa.

The mechanism was to introduce multiple aliphatic groups and an octane cyclosiloxane into the molecular design of thickeners. Carbon dioxide and lipid groups form hydrogen bonds through Lewis acid-base pairs [42–44]. The good chain flexibility of siloxane also plays a role in improving the solubility of the polymer in SC–CO_2 [35,45].

3.4.2. The Influence of Temperature on the Apparent Viscosity of HBD-1 and HBD-2 in SC–CO_2

The effect of temperature on the apparent viscosity of thickened SC–CO_2 was recorded in Figure 11. The results show that the apparent viscosity of the solution decreases with the increase in temperature. The results are the same as the previous studies on the effect of temperature on the apparent viscosity, because the temperature has a certain influence on the network structure of polymer chains [46–48]. The results also show that HBD-2 thickener has better temperature resistance when the temperature rises from 305.15 K to 315.15 K. This was because there are branched chains in HBD-2 polymer chains, and the polymer network structure can still maintain a certain tight network structure of the temperature action.

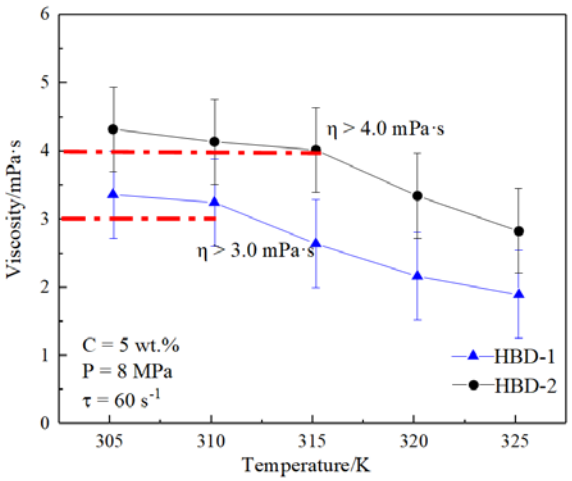

Figure 11. The influence of temperature on the apparent viscosity.

The mechanism was that when HBD polymer molecules enter SC–CO_2, the molecular chains entangle with each other in the form of curl, forming a complex three-dimensional

network structure. The molecular structure contains an eight-membered ring, and there are hydrogen bonds (carbonyl and CO_2) in the system [42–44], which hinder the flow of CO_2 molecules. When the initial temperature was low, the apparent viscosity decreased slowly. With the increase in temperature, the network structure was destroyed more and more thoroughly, and the apparent viscosity decreased sharply.

3.4.3. The Influence of Pressure on the Apparent Viscosity of HBD-1 and HBD-2 in SC–CO_2

Figure 12 records the response of pressure to the apparent viscosity of thickened SC–CO_2. The results show that the apparent viscosity of SC–CO_2 increases slowly from the increase in system pressure. According to the thickening mechanism, the intermolecular distance decreases to the increase in pressure, which makes it easier to form a more compact three-dimensional network structure [47]. In the process of pressurization, the self-winding of the polymer chain becomes closer, and the hydrogen bonding between the electron-donating group and CO_2 (Lewis acid-base formation) gradually increased [49], which was conducive to the increase in apparent viscosity. It can be seen from the study in Figure 12 that the viscosity increasing effect of HBD-2 was better than that of HBD-1 in the range of 7.48 MPa~14 MPa. It can be seen from Figure 12 that HBD-2 is more sensitive to pressure in the same pressure range. This is due to the existence of branched chains in the polymerization unit of HBD-2, and the network structure formed between the polymer molecules is more compact than that of HBD-1 after increasing the pressure. The denser network structure restricted the free flow of CO_2, and the viscosity of SC–CO_2 thickened by HBD-2 increased more obviously under the same pressure change. It was pointed out that the molecular design of thickeners can enrich branch chains in a certain range.

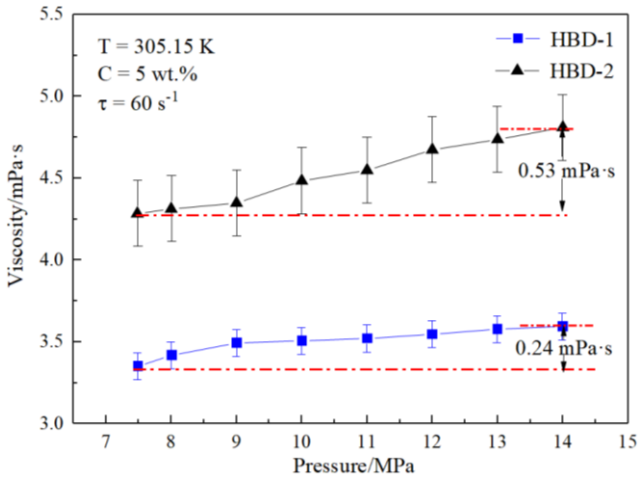

Figure 12. The influence of pressure on the apparent viscosity.

3.4.4. The Influence of Shear Rate on the Apparent Viscosity of HBD-1 and HBD-2 in SC–CO_2

Figure 13 shows the change in the apparent viscosity of SC–CO_2 after thickening in the shear rate range of 60 s^{-1} to 120 s^{-1}. Firstly, it can be seen from the figure that the change of shear rate does not affect the viscosity of pure CO_2, because pure CO_2 is a Newtonian fluid. HBD-1 and HBD-2 exhibit a negative correlation with shear rate, which proves that SC–CO_2 fluid after thickening is a power-law fluid with shear-thinning [43]. After thickening, the apparent viscosity of SC–CO_2 fluid decreases with the increase of shear rate, mainly because the increase of shear rate destroys the spatial network structure and restores the fluidity of CO_2 molecules that were originally restricted to flow.

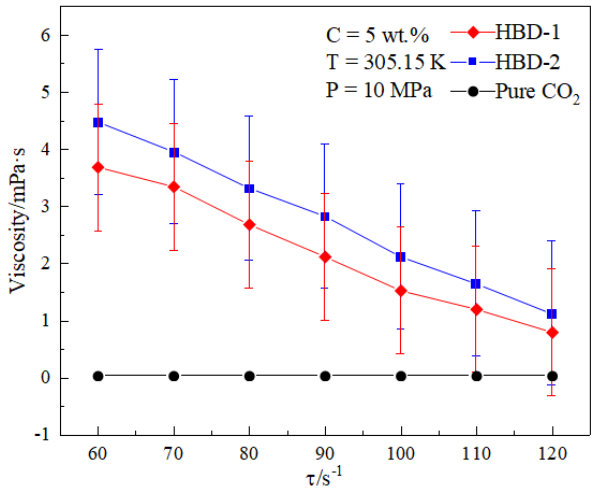

Figure 13. The influence of shear rate on the apparent viscosity.

3.4.5. The Influence of Thickener Content on the Apparent Viscosity of HBD-1 and HBD-2 in SC–CO_2

Figure 14 shows the effect of thickener content on the apparent viscosity of thickened SC–CO_2. The results show that the apparent viscosity increases in the range of 1 wt.%~5 wt.%. The mechanism of action was the number of polymer molecular chains that can form a tight network structure and hydrogen bonds in the system increased exponentially. Destroying these structures requires a lot of energy [50], and there is no external energy under experimental conditions. Therefore, the free-flowing SC–CO_2 molecules in the system were captured by the expanding polymer network, which shows the increase in apparent viscosity.

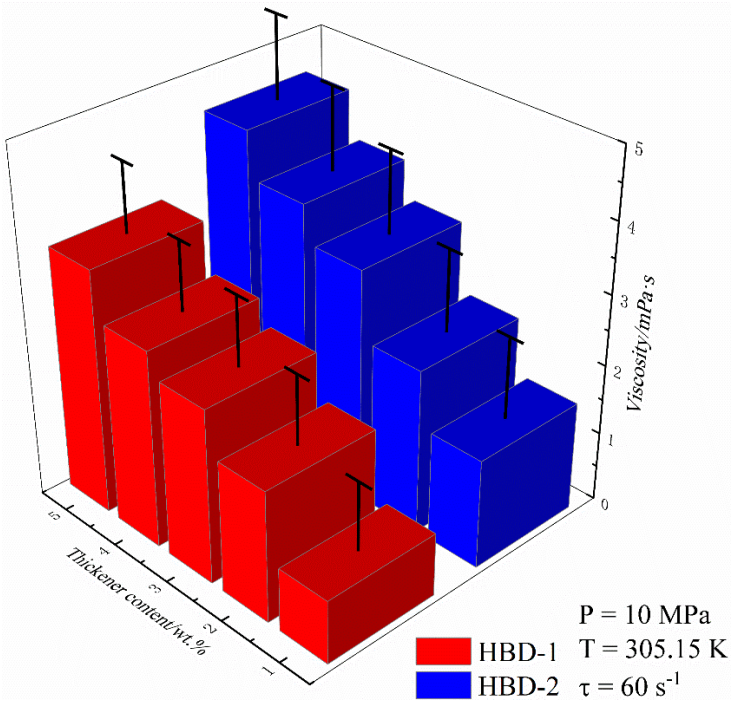

Figure 14. The influence of thickener content on the apparent viscosity.

3.5. Core Damage

In the development of oil and gas resources, there must be physical, biological, and thermal interactions between formation and fluid [51]. Air and water pollution caused

by traditional hydraulic fracturing were expected to be solved by SC–CO_2 water-free fracturing technology. In this study, a blank test was conducted first. The initial permeability measurement results are shown in Table 5.

Table 5. Initial permeability.

Type of Thickener	HBD-1			HBD-2		
Core number	1	2	3	4	5	6
Permeability/10^{-3} μm^2	14	18	20	13.4	12	13.6

The results show that the permeability of the core saturated with SC–CO_2 was the same as that of the core without SC–CO_2 immersion. Formation damage rates Equation (4) is shown as following:

$$\varphi = \frac{K_1 - K_2}{K_1} \times 100\% \quad (4)$$

where φ is formation damage rate, K_1 is matrix permeability before fracturing fluid injection ($\times 10^{-3}$ μm^2), K_2 is matrix permeability after fracturing fluid injection ($\times 10^{-3}$ μm^2).

Figure 15 shows the permeability loss rates of three cores with different permeability after fracturing with 5 wt.% HBD-1 and HBD-2 thickened SC–CO_2. The results show that each core has a certain degree of permeability loss, which shows that the core with higher permeability has less permeability loss and vice versa. This may be due to the fact that some thickeners adsorbed on the rock surface change the wettability, which leads to a decrease of permeability [52].

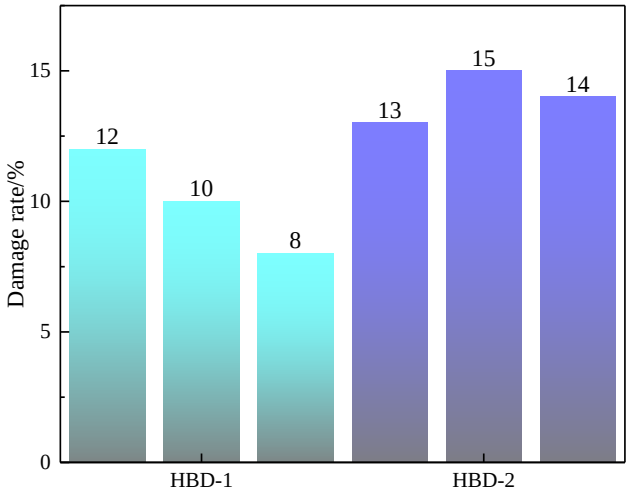

Figure 15. Core failure rate measurement results.

4. Conclusions

The SC–CO_2 thickener molecules HBD-1 and HBD-2 were designed by molecular simulation method, and the interaction energy, CED, and RDF of the thickener-CO_2 system were calculated. Using a self-designed and assembled capillary viscometer, the effects of content, temperature, shear rate, and pressure on the apparent viscosity of SC–CO_2 were studied. The excellent solubility of HBD-1 and HBD-2 thickeners was studied through simulation experiments and visualization experiments. The capillary viscometer was combined with a core displacement device to study the damage of thickened SC–CO_2 to the core. The results show that HBD-1 and HBD-2 (305.15 K, 7.48 MPa) have good solubility in SC–CO_2; the apparent viscosity of supercritical CO_2 fluid after thickening is positively related to pressure and dosage and is related to temperature and deceleration rate Negative correlation. HBD-2 has a better thickening effect at 5 wt.%, and the apparent viscosity can reach 4.48 mPa·s (305.15 K, 10 MPa).

There are three main mechanisms for polymer thickening and dissolution in SC–CO_2: polymer-polymer interaction, polymer-carbon dioxide interaction, and polymer chain flexibility. To avoid the use of fluoropolymers and co-solvents, following three mechanisms, the author introduced some CO_2-philic groups in the polymerization unit to increase the solubility of polymer molecules and introduced cyclic siloxanes to improve the viscosity-increasing effect. A thickener with good solubility in supercritical CO_2 was designed. This study verified the feasibility of this idea and found that the existence of multiple aliphatic groups in the branched-chain also had a certain impact on the viscosity, which opened up a new way for the development of environmentally friendly SC–CO_2 thickener.

Author Contributions: B.L. and Y.W. designed this experiment; B.L. performed a series of experiments about the preparation of this polymer and the effect of factors on the viscosity and rheology of the liquid CO2; B.L. and L.L. designed the capillary viscometer. All authors have read and agreed to the published version of the manuscript.

Funding: This investigation was supported by Joint Funds of the National Natural Science Foundation of China (U1762212).

Informed Consent Statement: Informed consent was obtained from all subjects involved in the study.

Data Availability Statement: The data presented in this study are available in the insert article.

Conflicts of Interest: The authors declare no conflict of interest.

Nomenclature

D4H 1:3,5,7-tetramethyl-l-cyclotetrasiloxane, HBD Hyperbranched D4H, T_g Glass transition temperature °C, τ Shear rate, s^{-1}.

References

1. Middleton, R.S.; Carey, J.W.; Currier, R.P.; Hyman, J.D.; Kang, Q.J.; Karra, S.; Jimenez-Martinez, J.; Porter, M.L.; Viswanathan, H.S. Shale gas and non-aqueous fracturing fluids: Opportunities and challenges for supercritical CO_2. *Appl. Energy* **2015**, *147*, 500–509. [CrossRef]
2. Middleton, R.S.; Gupta, R.; Hyman, J.D.; Viswanathan, H.S. The shale gas revolution: Barriers, sustainability, and emerging opportunities. *Appl. Energy* **2017**, *199*, 88–95. [CrossRef]
3. Sampath, K.H.S.M.; Perera, M.S.A.; Ranjith, P.G.; Matthai, S.K.; Rathnaweera, T.; Zhang, G.; Tao, X. CH4-CO2 gas exchange and supercritical CO2 based hydraulic fracturing as CBM production-accelerating techniques: A review. *J. CO2 Util.* **2017**, *22*, 212–230. [CrossRef]
4. Ao, X.; Lu, Y.Y.; Tang, J.R.; Chen, Y.T.; Li, H.L. Investigation on the physics structure and chemical properties of the shale treated by supercritical CO_2. *J. CO_2 Util.* **2017**, *20*, 274–281. [CrossRef]
5. Gordalla, B.C.; Ewers, U.; Frimmel, F.H. Hydraulic fracturing: A toxicological threat for groundwater and drinking-water. *Environ. Earth Sci.* **2013**, *70*, 3875–3893. [CrossRef]
6. Estrada, J.M.; Bhamidimarri, R. A review of the issues and treatment options for wastewater from shale gas extraction by hydraulic fracturing. *Fuel* **2016**, *182*, 292–303. [CrossRef]
7. Liu, M.; Shabaninejad, M.; Mostaghimi, P. Impact of mineralogical heterogeneity on reactive transport modelling. *Comput. Geosci.* **2017**, *104*, 12–19. [CrossRef]
8. Zhou, G.-G.; Chen, J.-G.; Wang, M.-X.; Zhang, M.; Guo, J.-L.; Shen, S.; Liu, Z.-T.; Liu, Z.-W.; Jiang, J.; Lu, J. Insight into the role of intermolecular interactions on the enhanced solubility of fluorinated epoxide oligomers in supercritical CO2. *Green Chem.* **2015**, *17*, 4489–4498. [CrossRef]
9. Desimone, J.; Guan, Z.; Elsbernd, C. Synthesis of fluoropolymers in supercritical carbon-dioxide. *Science* **1992**, *257*, 945. [CrossRef]
10. Huang, Z.; Shi, C.; Xu, J.; Kilic, S.; Enick, R.M.; Beckman, E.J. Enhancement of the viscosity of carbon dioxide using styrene/fluoroacrylate copolymers. *Macromolecules* **2000**, *33*, 5437–5442. [CrossRef]
11. Sun, B.; Sun, W.; Wang, H.; Li, Y.; Fan, H.; Li, H.; Chen, X. Molecular simulation aided design of copolymer thickeners for supercritical CO_2 as non-aqueous fracturing fluid. *J. CO_2 Util.* **2018**, *28*, 107–116. [CrossRef]
12. Wang, X.; Cheng, W.; Yang, Q.; Niu, H.; Liu, Q. Preliminary investigation on cytotoxicity of fluorinated polymer nanoparticles. *J. Environ. Sci.* **2017**. [CrossRef] [PubMed]
13. O'Brien, M.J.; Perry, R.J.; Doherty, M.D.; Lee, J.J.; Dhuwe, A.; Beckman, E.J.; Enick, R.M. Anthraquinone siloxanes as thickening agents for supercritical CO_2. *Energy Fuels* **2016**, *30*, 5990–5998. [CrossRef]
14. Du, M.; Sun, X.; Dai, C.; Li, H.; Wang, T.; Xu, Z.; Zhao, M.; Guan, B.; Liu, P. Laboratory experiment on a toluene-polydimethyl silicone thickened supercritical carbon dioxide fracturing fluid. *J. Pet. Sci. Eng.* **2018**, *166*, 369–374. [CrossRef]

15. Li, Q.; Wang, Y.; Li, Q.; Foster, G.; Lei, C. Study on the optimization of silicone copolymer synthesis and the evaluation of its thickening performance. *RSC Adv.* **2018**, *8*, 8770–8778. [CrossRef]
16. Wang, Y.; Li, Q.; Dong, W.; Li, Q.; Wang, F.; Bai, H.; Zhang, R.; Owusu, A.B. Effect of different factors on the yield of epoxy-terminated polydimethylsiloxane and evaluation of CO_2 thickening. *RSC Adv.* **2018**, *8*, 39787–39796. [CrossRef]
17. Li, Q.; Wang, Y.; Wang, X.; Yu, H.; Li, Q.; Wang, F.; Bai, H.; Kobina, F. An application of thickener to increase viscosity of liquid CO_2 and the assessment of the reservoir geological damage and CO_2 utilization. *Energy Sources Part A Recovery Util. Environ. Eff.* **2019**, *41*, 368–377.
18. Llave, F.M.; Chung, T.H.; Burchfield, T.E. Use of entrainers in improving mobility control of supercritical CO sub 2. *SPE Reserv. Eng.* **1990**, *5*, 47–51. [CrossRef]
19. Zhang, S.; She, Y.; Gu, Y. Evaluation of polymers as direct thickeners for CO_2 enhanced oil recovery. *J. Chem. Eng. Data* **2011**, *56*, 1069–1079. [CrossRef]
20. Hu, D.; Sun, S.; Yuan, P.; Zhao, L.; Liu, T. Evaluation of CO2-philicity of poly(vinyl acetate) and poly(vinyl acetate-alt-maleate) copolymers through molecular modeling and dissolution behavior measurement. *J. Phys. Chem. B* **2015**, *119*, 3194–3204. [CrossRef]
21. Hu, D.; Sun, S.; Yuan, P.-Q.; Zhao, L.; Liu, T. Exploration of CO2-philicity of poly(vinyl acetate-co-alkyl vinyl ether) through molecular modeling and dissolution behavior measurement. *J. Phys. Chem. B* **2015**, *119*, 12490–12501. [CrossRef]
22. Hu, D.; Zhang, Y.; Su, M.; Bao, L.; Zhao, L.; Liu, T. Effect of molecular weight on CO2-philicity of poly(vinyl acetate) with different molecular chain structure. *J. Supercrit. Fluids* **2016**, *118*, 96–106. [CrossRef]
23. Guo, D.J.; Han, H.M.; Jing, W.; Xiao, S.J.; Dai, Z.D. Surface-hydrophilic and protein-resistant silicone elastomers prepared by hydrosilylation of vinyl poly(ethylene glycol) on hydrosilanes-poly(dimethylsiloxane) surfaces. *Colloids Surf. A Physicochem. Eng. Asp.* **2007**, *308*, 129–135. [CrossRef]
24. Girard, E.; Tassaing, T.; Ladavière, C.; Marty, J.-D.; Destarac, M. Distinctive features of solubility of RAFT/MADIX-derived partially trifluoromethylated poly(vinyl acetate) in supercritical CO2. *Macromolecules* **2012**, *45*, 9674–9681. [CrossRef]
25. Birkin, N.A.; Wildig, O.J.; Howdle, S.M. Effects of poly(vinyl pivalate)-based stabiliser architecture on CO2-solubility and stabilising ability in dispersion polymerisation of N-vinyl pyrrolidone. *Polym. Chem.* **2013**, *4*, 3791–3799. [CrossRef]
26. Tarhan, İ. A comparative study of ATR-FTIR, UV–visible and fluorescence spectroscopy combined with chemometrics for quantification of squalene in extra virgin olive oils. *Spectrochim. Acta Part A Mol. Biomol. Spectrosc.* **2020**, *241*, 118714. [CrossRef] [PubMed]
27. Batzer, H.; Zahir, S.A.C. Studies in the molecular weight distribution of epoxide resins. I. Gel permeation chromatography of epoxide resins. *J. Appl. Polym. Sci.* **1975**, *19*, 585–600. [CrossRef]
28. Tan, B.; Bray, C.L.; Cooper, A.I. Fractionation of poly(vinyl acetate) and the phase behavior of end-group modified oligo(vinyl acetate)s in CO2. *Macromolecules* **2009**, *42*, 7945–7952. [CrossRef]
29. Zhang, S.; Luo, Y.; Yang, H.; Yang, H.-J.; Tan, B. Functional oligo(vinyl acetate) bearing bipyridine moieties by RAFT polymerization and extraction of metal ions in supercritical carbon dioxide. *Polym. Chem.* **2013**, *4*, 3507–3513. [CrossRef]
30. Jennings, J.; Bassett, S.P.; Hermida-Merino, D.; Portale, G.; Bras, W.; Knight, L.; Titman, J.J.; Higuchi, T.; Jinnai, H.; Howdle, S.M. How does dense phase CO2 influence the phase behaviour of block copolymers synthesised by dispersion polymerisation? *Polym. Chem.* **2016**, *7*, 905–916. [CrossRef]
31. Cummings, S.; Xing, D.; Enick, R.; Rogers, S.; Heenan, R.; Grillo, I.; Eastoe, J. Design principles for supercritical CO2 viscosifiers. *Soft Matter* **2012**, *8*, 7044–7055. [CrossRef]
32. Aycaguer, A.-C.; Lev-On, M.; Winer, A.M. Reducing carbon dioxide emissions with enhanced oil recovery projects: A Life cycle assessment approach. *Energy Fuels* **2001**, *15*, 303–308. [CrossRef]
33. Raveendran, P.; Wallen, S.L. Sugar acetates as novel, renewable CO(2)-philes. *J. Am. Chem. Soc.* **2002**, *124*, 7274–7275. [CrossRef] [PubMed]
34. Marcus, Y. Are solubility parameters relevant to supercritical fluids? *J. Supercrit. Fluids* **2006**, *38*, 7–12. [CrossRef]
35. Defelice, J.; Lipson, J.E.G. Polymer miscibility in supercritical carbon dioxide: Free volume as a driving force. *Macromolecules* **2014**, *47*, 5643–5654. [CrossRef]
36. Lee, H.; Pack, J.W.; Wang, W.; Thurecht, K.J.; Howdle, S.M. Synthesis and phase behavior of CO2-soluble hydrocarbon copolymer: Poly(vinyl acetate-alt-dibutyl maleate). *Macromolecules* **2010**, *43*, 2276–2282. [CrossRef]
37. Gestoso, P.; Brisson, J. Towards the simulation of poly(vinyl phenol)/poly(vinyl methyl ether) blends by atomistic molecular modelling. *Polymer* **2003**, *44*, 2321–2329. [CrossRef]
38. Fu, Y.; Liao, L.; Yang, L.; Lan, Y.; Mei, L.; Liu, Y.; Hu, S. Molecular dynamics and dissipative particle dynamics simulations for prediction of miscibility in polyethylene terephthalate/polylactide blends. *Mol. Simul.* **2013**, *39*, 415–422. [CrossRef]
39. Gnanasambandam, R.; Proctor, A. Determination of pectin degree of esterification by diffuse reflectance Fourier transform infrared spectroscopy. *Food Chem.* **2000**, *68*, 327–332. [CrossRef]
40. Drohmann, C.; Beckman, E.J. Phase behavior of polymers containing ether groups in carbon dioxide. *J. Supercrit. Fluids* **2002**, *22*, 103–110. [CrossRef]
41. Malhotra, S.L.; Lessard, P.; Blanchard, L.P. The thermal decomposition and glass transition temperature of poly(p-tert-butyistyrene). *J. Macromol. Sci. Part A Chem.* **2012**, *15*, 121–141. [CrossRef]
42. Gu, Y.; Kar, T.; Scheiner, S. Fundamental properties of the CH···O interaction: Is it a true hydrogen bond? *J. Am. Chem. Soc.* **1999**, *121*, 9411–9422. [CrossRef]

43. Raveendran, P.; Wallen, S.L. Cooperative C-H···O hydrogen bonding in CO_2—lewis base complexes: Implications for solvation in supercritical CO_2. *J. Am. Chem. Soc.* **2002**, *124*, 12590–12599. [CrossRef] [PubMed]
44. Ginderen, P.; Herrebout, W.; van der Veken, B. van der Waals complex of dimethyl ether with carbon dioxide. *J. Phys. Chem. A* **2003**, *107*, 5391–5396. [CrossRef]
45. Rindfleisch, F.; Dinoia, T.P.; McHugh, M.A. Solubility of polymers and copolymers in supercritical CO2. *J. Phys. Chem.* **1996**, *100*, 15581–15587. [CrossRef]
46. Bae, J.H.; Irani, C.A. A laboratory investigation of viscosified CO2 process. *SPE Adv. Technol.* **1993**, *1*, 166–171. [CrossRef]
47. Luo, X.; Wang, S.; Wang, Z.; Jing, Z.; Lv, M.; Zhai, Z.; Han, T. Experimental investigation on rheological properties and friction performance of thickened CO2 fracturing fluid. *J. Pet. Sci. Eng.* **2015**, *133*, 410–420. [CrossRef]
48. Doherty, M.D.; Lee, J.J.; Dhuwe, A.; O'Brien, M.J.; Perry, R.J.; Beckman, E.J.; Enick, R.M. Small molecule cyclic amide and urea based thickeners for organic and SC–CO2/organic solutions. *Energy Fuels* **2016**, *30*, 5601–5610. [CrossRef]
49. Kilic, S.; Michalik, S.; Wang, Y.; Johnson, J.K.; Enick, R.M.; Beckman, E.J. Effect of grafted lewis base groups on the phase behavior of model poly(dimethyl siloxanes) in CO_2. *Ind. Eng. Chem. Res.* **2003**, *42*, 6415–6424. [CrossRef]
50. Tsukahara, T.; Kayaki, Y.; Ikariya, T.; Ikeda, Y. 13C NMR spectroscopic evaluation of the affinity of carbonyl compounds for carbon dioxide under supercritical conditions. *Angew. Chem. Int. Ed.* **2004**, *43*, 3719–3722. [CrossRef]
51. Reinicke, A.; Rybacki, E.; Stanchits, S.; Huenges, E.; Dresen, G. Hydraulic fracturing stimulation techniques and formation damage mechanisms—Implications from laboratory testing of tight sandstone–proppant systems. *Geochemistry* **2010**, *70*, 107–117. [CrossRef]
52. Civan, F. *Reservoir Formation Damage*; Gulf Professional Pub.: Houston, TX, USA, 2007.